

Radiation Damage Study for PHENIX Silicon Stripixel Sensor

J. Asai^a, S. Batsouli^b, K. Boyle^c, V. Castillo^d, V. Cianciolo^b, D. Fields^e,
Y. Hosoi^f, R. Ichimiya^a, Y. Inoue^f, M. Kawashima^f, T. Komatsubara^g,
K. Kurita^f, Z. Li^h, M. Nguyen^c, T. Murakamiⁱ, R. Nouicer^j,
H. Ohnishi^a, R. Pak^j, K. Sakashita^k, K. Suga^f, A. Taketani^a, J. Tojo^a

^a *RIKEN (The Institute of Physical and Chemical Research), Wako, Saitama 351-0198, Japan*

^b *Oak Ridge National Laboratory, Oak Ridge, TN 37831, USA*

^c *Department of Physics and Astronomy, Stony Brook University, Stony Brook, NY 11794-3800, USA*

^d *Brookhaven National Laboratory, C-A Department, Upton, NY 11973-5000, USA*

^e *University of New Mexico, Albuquerque, NM 87131, USA*

^f *Rikkyo University, Toshima, Tokyo 171-8501, Japan*

^g *Institute of Physics and Tandem Accelerator Center, University of Tsukuba, Tsukuba, Ibaraki, 305-8577, Japan*

^h *Brookhaven National Laboratory, Instrumentation Division, Upton, NY 11973-5000, USA*

ⁱ *Department of Physics, Kyoto University, Kyoto, Kyoto, 606-8502, Japan*

^j *Brookhaven National Laboratory, Chemistry Department, Upton, NY 11973-5000, USA*

^k *Tokyo Institute of Technology, Meguro, Tokyo 152-8551, Japan*

Abstract

Silicon stripixel sensors which were developed at BNL will be installed as part of the RHIC-PHENIX silicon vertex tracker (VTX). RHIC II operations provide luminosity up to $2 \times 10^{32} \text{ cm}^{-2} \text{ s}^{-1}$ so the silicon stripixel sensors will be exposed to a significant amount of radiation. The most problematic radiation effect for VTX is the increase of leakage current, which degrades the signal to noise ratio and may saturate the readout electronics.

We studied the radiation damage using the same diodes as CERN-RD48. First, the proportionality between the irradiation fluence and the increase of leakage current of CERN-RD48 was reproduced. Then beam experiments with stripixel sensor were done in which leakage current was found to increase in the same way as that of the reference diode.

A stripixel sensor was also irradiated at the PHENIX interaction region (IR) during the 2006 run. We found the same relation between the integrated luminosity and determined fluence from increase of leakage current. The expected fluence is $3\text{-}6 \times 10^{12} \Phi_{eq}/\text{cm}^2$ (1 MeV neutron equivalent) in RHIC II operations for 10 years. Due to this expected exposure, setting the operating temperature in PHENIX to $T \leq 0^\circ \text{C}$ to suppress leakage current is needed to avoid saturation of preamplifiers.

1. Introduction

The PHENIX experiment (1) at the Relativistic Heavy Ion Collider (RHIC) at Brookhaven National Laboratory (BNL) has been successful in investigating new forms of matter in heavy-ion reactions and the spin structure of the nucleon in polarized p+p collisions at highly relativistic energies.(2) However, the current PHENIX detector configuration has limited capability in identifying heavy quarks and parton jets. These probes are important for understanding heavy ion and spin physics. The PHENIX VTX upgrade can enhance the physics from those channels.

Efficient topological reconstruction of open charm decays requires a good tracking 'point-back' resolution to the primary collision vertex. Further, the beam pipe and innermost layers of detector must be very thin and as close to the beam as possible to allow measurement of particles at low transverse momentum, which comprise the bulk of the cross section. A thin beam pipe and inner detector layers are also key elements in efficiently vetoing photon conversion electrons, which in combination with electron identification from the PHENIX central-arm spectrometer ($|\eta| < 0.35$) will enable much improved measurement of heavy quark weak decays. Sensitivity of the present combined measurements of bottom and charm quarks will be improved by the central silicon vertex tracker (3), which will allow us to separate charm and bottom quarks, in addition to separating them from light flavor quarks.

In the QCD picture, the proton is made from valence quarks, a sea of the quark-antiquark pairs and gluons. The spin of the proton should be explained by the sum of spin of quarks and gluons, and their orbital angular momentum. The contribution from quark spin has been measured by the polarized lepton deep inelastic scattering experiment (DIS). However this explains only 20% of the proton spin. Since the gluons can not interact with leptons, DIS is not the best way to investigate gluon contributions. Therefore polarized p+p collisions use gluons and quarks as probes to interact with gluons. In PHENIX, we have measured the double longitudinal-spin asymmetry A_{LL} of π^0 production in polarized p+p collisions (4). In this process, π^0 carries only a fraction of the momentum of the scattering quark or gluon. More direct information of the gluon polarization will be obtained by measuring A_{LL} of direct-photon and heavy quark production using the PHENIX central-arm spectrometer and the central silicon vertex tracker.

The central silicon vertex tracker consists of four layers of barrel detectors, and covers 2π azimuthal angle and $|\eta| < 1.2$. The inner two layers are silicon pixel detectors and the outer two layers are silicon stripixel detectors, composed of 246 stripixel sensors. The radial distances of the barrel shaped layers from the colliding beam are 2.5 cm, 5 cm, 10 cm and 14 cm. Fig. 1 illustrates the planned layout for the VTX upgrade. Due to close proximity of VTX to interaction point, the detector and electronics will be harshly irradiated in the PHENIX environment. (luminosity of RHIC II operations

Email address: kurita@ne.rikkyo.ac.jp (K. Kurita).

will be $2 \times 10^{32} \text{ cm}^{-2} \text{ s}^{-1}$). In this paper, the study of the effect on the PHENIX vertex stripixel sensor used in the third and fourth layers will be discussed.

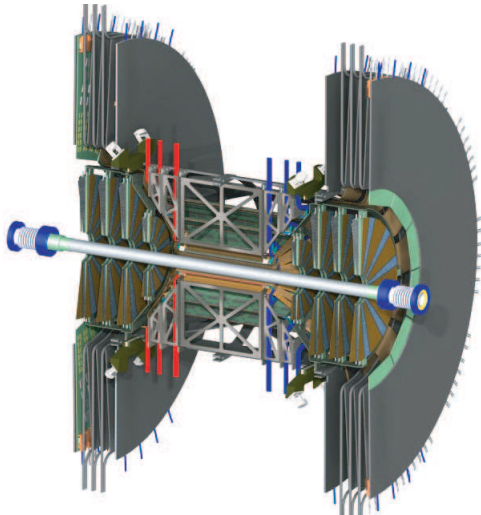


Fig. 1. Layout of PHENIX silicon vertex tracker (VTX).

2. Silicon stripixel sensor

A novel stripixel silicon sensor has been developed at BNL. (5) The silicon sensor is a single-sided, DC-coupled, two dimensional (2D) sensitive detector. This design is simpler for sensor fabrication and signal processing than the conventional double-sided strip sensor. Each pixel from the stripixel sensor is made from two interleaved implants (a-pixel and b-pixel) in such a way that the charge deposited by ionizing particles can be seen by both implants as presented in Fig. 2.A. The a-pixels are connected to form a X-strip as is presented in Fig. 2.B. The b-pixels are connected in order to form a U-strip as is presented in Fig. 2.C. The stereo angle between a X-strip and a U-strip is 4.6° . In 2005, mask design and processing technology was transferred successfully from BNL to sensor fabrication company Hamamatsu Photonics (HPK) located in Japan, for mass production. The stripixel sensor specifications are summarized in Table 1. The readout side is implanted with p-type ions and the back side is implanted with n-type ions. It allows compact arrangement without connecting electronics in the back.

A stripixel sensor is wire-bonded to twelve SVX4 ASIC (6) chips each having 128 channels. The SVX4 ASIC originally developed by Fermi National Accelerator Laboratory and Berkeley National Laboratory was designed for use as an AC-coupled device. But we chose DC-couple between the stripixel sensor and SVX4 to take advantage of the higher S/N ratio. However, the SVX4 preamplifier may saturate from the leakage current. The preamplifier has a dynamic range of 200 fC and must be reset during a series of unfilled beam bunches which come every $13 \mu\text{sec}$ at RHIC. This limits the leakage current to 15 nA/strip. Under these conditions signal-to-noise ratio in the detector was found to

Table 1
Stripixel sensor properties.

Diode configuration	p+/n/n+
Resistivity	4-10 k Ω
Sensor size	3.43 x 6.36 [cm ²]
Sensitive area	3.072 x 3.000 x 2 [cm ²]
Thickness	625 [μ m]
Pixel structure	Spiral structure 5 μ m line, 3 μ m gap
Effective pixel size	80 x 1000 [μ m ²]
Strip construction	Chain of 30 pixels
Number of Strips	Total: 1536 X-strip: 384 x 2, U-strip: 384 x 2
Readout	DC coupled
Front-end electronics	SVX4 ASIC

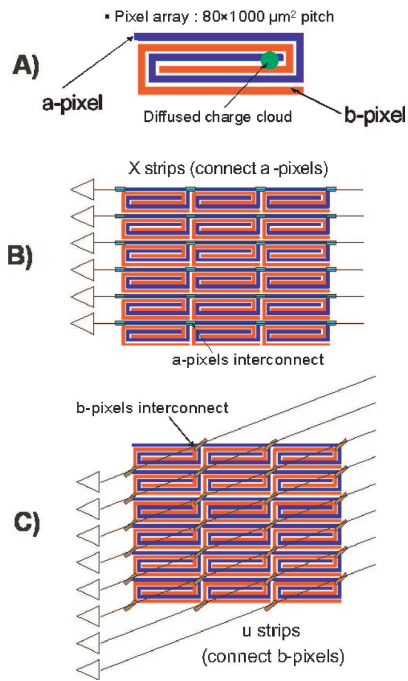


Fig. 2. Layout of the stripixel sensor.

be better than 20:1. Although the first layer of VTX is exposed to the highest radiation, the pixel detectors are read out by AC-coupled electronics, thus there is no concern about saturation. Therefore, the increase of leakage current is the most problematic radiation effect for the stripixel detectors. To estimate the leakage current accurately, actual silicon

stripixel sensors were irradiated and their leakage currents were measured.

3. Radiation damage effect of silicon sensor

There are three known radiation effects on a silicon sensor: (1) increase of leakage current due to generation of point defects; (2) decrease of charge collection efficiency due to induced trapping centers; and (3) change of depletion voltage due to increase of effective acceptor density. Among the three radiation effects listed, the most problematic effect for our application is (1) increase of leakage current, because the leakage current which can flow into the DC-coupled charge sensitive preamplifier is limited to 15 nA/channel. Therefore, we will hereafter focus our discussion on the effect of the leakage current.

Extensive study done by CERN-RD48 has found the following relation between increase of leakage current and 1 MeV neutron equivalent fluence Φ_{eq} :

$$\Delta I/Volume = \alpha\Phi_{eq} \quad (1)$$

where ΔI is the difference in leakage current before and after irradiation and α is the proportionality factor called the current related damage rate.(9) A typical value of α after post-irradiation annealing is 4×10^{-17} A/cm. Eq. (1) was used as a guide throughout our experimental study.

3.1. Determination of increase of leakage current, ΔI

The leakage current I depends on the thickness of the depletion layer d , and increases with increasing voltage V as:

$$I \propto d \propto \sqrt{V}. \quad (2)$$

ΔI is determined by the difference between pre-irradiation leakage current and post-annealing leakage current measured at full depletion voltage, V_{FD} .(7) The capacitance C decreases with increasing voltage V as:

$$C \propto 1/\sqrt{V}. \quad (3)$$

At full depletion, C reaches its minimum. V_{FD} is determined graphically using the bias voltage dependence of $1/C^2$ as shown in Fig. 5.

Leakage current also depends on the temperature T [K] as:

$$I \propto T^2 \exp(-E_g/2k_B T) \quad (4)$$

where, E_g is the energy gap of silicon ($E_g = 1.2$ eV); and k_B is the Boltzman constant ($k_B = 8.6 \times 10^{-5}$ eV/K). This relation holds for any silicon sensor both before and after irradiation. Most of our measurements are done at 20 °C, otherwise for comparison the leakage current readings were converted to 20 °C equivalent value using Eq. (4). Therefore, the leakage current can be controlled to some extent by adjusting the operating temperature. This relation will be used to evaluate the operating temperature for VTX in RHIC II running conditions.

In our study of silicon sensor properties, the dependences of capacitance and leakage current on bias voltage were measured. The circuit diagram of the measurement system is shown in Fig. 3. Bias voltage was applied from the back of the sensors, and capacitance and leakage current were measured through readout pads. The system consists of a

picoammeter/voltage source (Keithley 6487), a LCR meter (HP 4263 B) and a switch scanner system (Keithley 7002), controlled by LabVIEW through a GPIB interface.

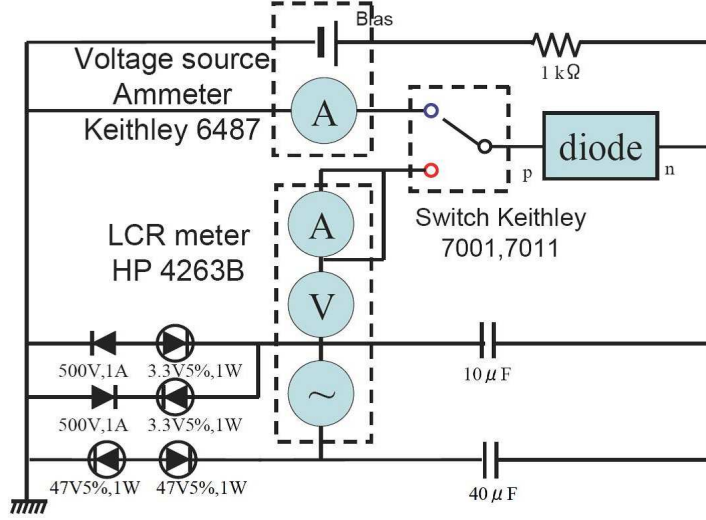


Fig. 3. Measurement system circuit diagram.

The current related damage rate α is determined by the temperature history after the start of irradiation.(9) The dependence is described as

$$\alpha(t) = \alpha_I \exp(-t/\tau_I(T)) + \alpha_0(T) - \beta \ln(t/t_0) \quad (5)$$

where t is the time from the irradiation time [min]; T is the temperature; $\alpha_I = 1.23 \times 10^{-17}$ [A/cm]; $\beta = 3.07 \times 10^{-18}$ [A/cm]; $t_0 = 1$ [min];

$$1/\tau_I = \kappa_{0I} \times \exp(-E_I/\kappa_B T) \quad (6)$$

where $\kappa_{0I} = 1.2 \times 10^{13}$ [s⁻¹] and $E_I = 1.11$ [eV];

$$\alpha_0 = -8.9 \times 10^{-17} [\text{A/cm}] + 4.6 \times 10^{-14} [\text{AK/cm}] \times 1/T. \quad (7)$$

4. Detemination of neutron equivalent fluence, Φ_{eq}

Radiation leads to point defects in Si. The displacement damage by different particles causes various levels of defects. For a quantitative study of this effect on the silicon sensor, it is necessary to know the type and the energy of the radiation particle as well as its fluence. The conversion factor known as the hardness factor κ evaluated by the Non-Ionizing Energy Loss (NIEL) hypothesis is plotted in Fig. 4 as a function of energy for neutrons, protons, pions and electrons.(8) The following equation was used to convert beam fluence Φ_{beam} to 1 MeV neutron equivalent Φ_{eq} :

$$\Phi_{eq} = \kappa \Phi_{beam}. \quad (8)$$

A method to monitor Φ_{eq} with reference diodes will now be described.

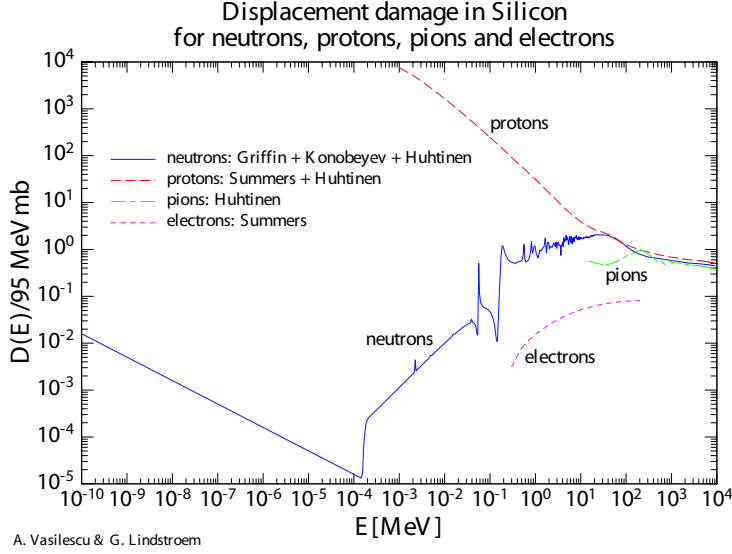


Fig. 4. Hardness factor distribution. (8)

4.1. Beam test with reference diode

The diodes which we used for beam irradiation tests were the same kind developed by CERN-RD48 collaboration. Denoting as "reference diode", its properties are listed in Table 2. For the electrical measurements, the reference diodes of CERN-RD48 type were mounted on a printed circuit board (PCB) with bias and signal lines connected through Lemo connectors. The guard ring on the front of the diode was wire-bonded to GND, and bias voltage was applied on its back via conductive epoxy glue, which held the diode in place. The front charge collection electrode inside the guard ring was wire-bonded to one of the connectors, and was readout by the setup shown in Fig. 3 before and after irradiation. Another diode used for confirmation purposes was Si PIN photodiode S3204-08 from Hamamatsu Photonics. Its properties are also listed in Table 2.

In order to cover a wide range of fluence, irradiation experiments were performed at two complementary facilities, namely the Cockcroft-Walton accelerator at Rikkyo University for the low fluence measurements, and the Tandem Van de Graaff accelerator at Kyoto University for the high fluence measurements. Rikkyo Cockcroft-Walton accelerator provides low intensity 14 MeV neutrons from deuteron-triton fusion reactions, and is suited for low fluence measurement. However, to reach $\Phi_{eq} > 10^{11}/\text{cm}^2$ is time prohibitive. On the other hand, Kyoto Tandem can provide an intense 12 MeV proton beam of the order of 1 nA ($\sim 10^{10}$ particles/s), but transport becomes unstable below this beam current, making an accurate fluence measurement below $10^{11}/\text{cm}^2$ difficult.

We investigated the correspondence between beam monitor fluences and diode fluences as follows. For the 14 MeV neutron beam from the Cockcroft-Walton accelerator at Rikkyo, the fluences were between 1×10^{10} and $1 \times 10^{11} N_{eq}/\text{cm}^2$. The beam fluence was estimated from TPS-452BS neutron counter from ALOKA. The hardness factor of 14 MeV neutron is 1.823 ± 0.006 . The diode fluence was estimated through an increase of leakage current. The current related damage rate α was estimated using temperature

Table 2
Reference diode properties.

Diode type	Diode configuration	Resistivity [k Ω]	Active area [cm ²]	Thickness [cm]	Volume [cm ³]
CERN-RD48	p ⁺ /n/n ⁺	2	2.5 $\times 10^{-1}$	3.04 $\times 10^{-2}$	7.6 $\times 10^{-3}$
S3204-08	PIN	-	3.24	3 $\times 10^{-2}$	9.7 $\times 10^{-2}$

history of temperature logger data. Fig. 5 shows the IV and CV measurements, where the leakage current and capacitance were measured before irradiation and after annealing, and the annealing was done at 60 °C for 80 min. The increase of leakage current is calculated between pre-irradiation (black points) and post-annealing (blue points) at V_{FD} (dashed line), while the red points are the measured result post-irradiation. The resulting distribution is shown in Fig. 6. The agreement was well established. For the 12 MeV proton beam at Kyoto Tandem, the beam fluence was estimated from a Faraday cup measurement. The hardness factor of 12 MeV protons is 3.6 ± 0.1 . The fluences of diodes were estimated by the same method as that of 14 MeV neutron beam tests. Our final results are shown in Fig. 6, which agree with beam monitor values within 25%. The details of irradiation results are summarized in Table 3.

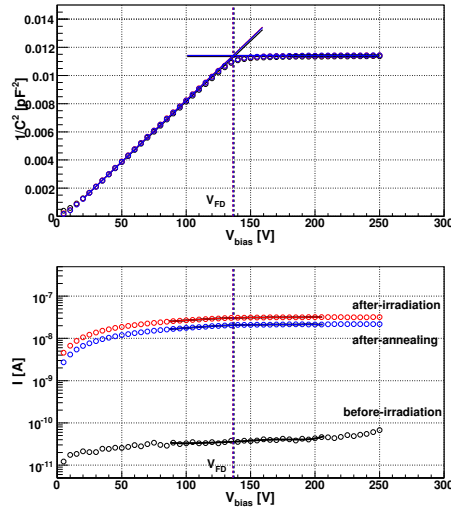


Fig. 5. Electrical measurements for the reference diode irradiated by a 14 MeV neutron beam with fluence of $\Phi_{eq}=6.6 \times 10^{10}$ [N_{eq}/cm²].

4.2. Temperature dependence of reference diode

We studied the temperature dependence of leakage current with the reference diode which had been irradiated by 12 MeV proton beam with $\Phi_{eq}=5.79 \times 10^{12}$ [N_{eq}/cm²] at Kyoto Univ. The diodes were measured at 5 °C intervals from 0 °C to 30 °C. The ratio of the leakage current is shown in Fig. 7, where the red curve represents the calculation using Eq. (4) normalized to 20 °C. The temperature dependence of the leakage current

Table 3

Beam test result with reference diodes.

Beam particle	neutron	neutron	proton	proton	proton	proton
Beam energy [MeV]	14	14	12	12	12	12
Diode type	S3204-08	CERN-RD48	CERN-RD48	CERN-RD48	CERN-RD48	CERN-RD48
$\Delta I/\text{Volume}$ [A/cm ³]	6.42×10^{-7}	2.66×10^{-6}	3.06×10^{-5}	1.98×10^{-4}	2.73×10^{-4}	5.08×10^{-4}
Error $\Delta I/\text{Volume}$ [A/cm ³]	8.74×10^{-9}	7.58×10^{-8}	8.88×10^{-8}	5.96×10^{-7}	1.89×10^{-7}	8.88×10^{-7}
α [A/cm]	4.00×10^{-17}	4.05×10^{-17}	4.11×10^{-17}	4.09×10^{-17}	4.12×10^{-17}	4.19×10^{-17}
Diode fluence [N_{eq}/cm^2]	1.60×10^{10}	6.57×10^{10}	7.44×10^{11}	4.85×10^{12}	6.63×10^{12}	1.21×10^{13}
Error diode fluence [N_{eq}/cm^2]	2.71×10^8	1.87×10^9	8.64×10^9	5.85×10^{10}	1.85×10^{10}	8.47×10^{10}
Beam fluence [$/\text{cm}^2$]	1.42×10^{10}	4.96×10^{10}	1.53×10^{11}	1.55×10^{12}	1.59×10^{12}	3.20×10^{12}
Hardness factor κ	1.823	1.823	3.6	3.6	3.6	3.6
Beam fluence [N_{eq}/cm^2]	2.58×10^{10}	9.04×10^{10}	5.56×10^{11}	5.62×10^{12}	5.79×10^{12}	1.16×10^{13}

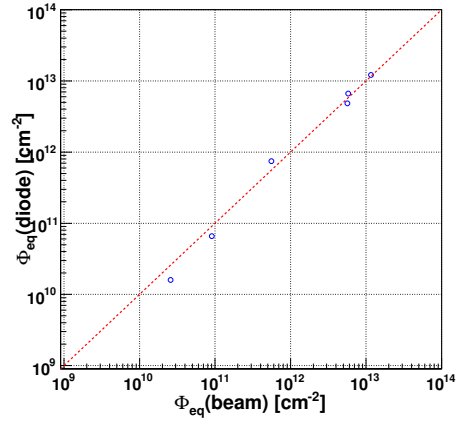


Fig. 6. Comparison of fluence from reference diode and beam information.

agrees with Eq. (4) within less than 18% error. Therefore the increase of leakage current of the stripixel sensor from radiation damage in RHIC II operations can be offset by lowering the operating temperature environment regardless of saturation of the circuit.

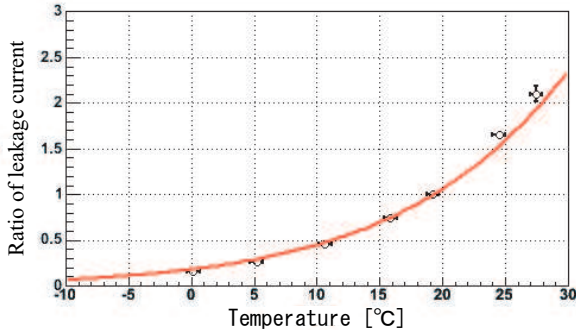


Fig. 7. Temperature dependence of leakage current for irradiated diode.

5. Beam irradiation test of stripixel sensor

The radiation damage test results of the stripixel sensors are described in this section. In preparation for the tests, we designed a PCB for the stripixel sensor. The PCB had a rectangular opening which was slightly bigger than the sensitive area of the stripixel sensor. A stripixel sensor was glued on the PCB in such a way that the sensitive area was centered in the opening. The PCB had 24 single readout, bias, GND and signal sum readout connectors. The guard ring on the front surface of the stripixel sensor was wire-bonded to the GND connector. The bias was supplied from the back side of the sensor. A sample of 24 strips out of 1536 strips was wire-bonded to individual readout connectors and the rest of the strips were wire-bonded together to the signal sum readout connector. This arrangement allowed measurement of the individual strips of the pre-selected sample as well as total leakage current when the 24 individual readout channels were externally connected with the signal sum channel. Before the beam irradiation tests, stripixel sensors were mounted on the PCB and pre-irradiation leakage current measurements were done. We also measured the capacitance of the stripixel sensor. The annealing was done at 60 °C for 80 minutes. The increase of leakage current was estimated at 20 °C. The current related damage rate α was determined from the temperature history recorded by a temperature logger, which was installed in the same setup.

In order to determine the fluence dependence of leakage current, we made measurements at two different fluence settings. We used 14 MeV neutron from deuteron-triton fusion reaction for the low fluence test at Rikkyo and 16 MeV proton beam for the high fluence test at the Tandem Accelerator Center in the University of Tsukuba. Tsukuba Tandem was chosen because its proton beam energy was high enough to penetrate the 625 μm thick stripixel sensor without significant energy loss, which affects the hardness factor.

5.1. Beam irradiation test setup

The setup of 14 MeV neutron irradiation test at Rikkyo Univ. is shown in Fig. 8. Due to the fact that neutrons do not have ionization energy loss, the experimental arrangement was rather trivial. The stripixel sensor, a reference diode and the TPS-451BS neutron counter were placed behind the tritium target in line with the incoming deuteron beam.

The beam current on the target was monitored for the beam stability control. The pulse output of the neutron counter was sent to the control room and counted by a scaler to obtain the neutron fluence.

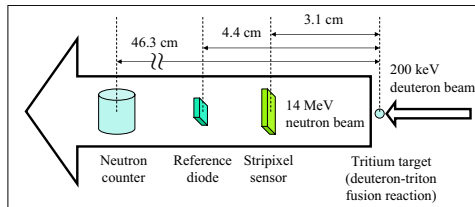


Fig. 8. Beam test setup with 14 MeV neutrons.

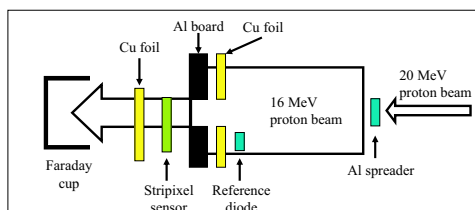


Fig. 9. Beam test setup with 16 MeV protons.

In the case of proton irradiation test, it is necessary to avoid localization in beam experiments to simulate almost uniform irradiation in the actual PHENIX environment. The setup of the 16 MeV proton irradiation test at Univ. of Tsukuba is shown in Fig. 9. The original 20 MeV proton beam from the Tandem Van de Graaff accelerator was spread with a 0.5 mm thick aluminum plate by Coulomb multiple scattering. The standard deviation of the spread was 3.8 cm at the sensor under test. The energy of the beam after the spreader is also affected and the mean value energy of the beam was 16 MeV. An aluminum collimator plate of 5 mm thickness was placed 150 cm downstream of the spreader. The Al collimator had a square opening of the size $30 \times 30 \text{ mm}^2$ which was aligned to the center of the beam. A Cu foil was mounted in front of the collimator and it had the same opening so that the beam directly entered the stripixel sensor. The Al collimator size was $200 \times 150 \text{ mm}^2$ to cover the PCB. One full stripixel pattern of the sensor was irradiated with 16 MeV proton spread beam through the opening of the collimator. A reference diode was placed by the side of the stripixel sensor on the front Cu foil. A Faraday cup was used for the beam fluence monitor at the end of the beam line. A magnetic field was applied to the cup to sweep away escaping secondary electrons.

5.2. Fluence determination

The fluence at the stripixel sensor position was estimated from the reference diode, which was irradiated together with the stripixel sensor. In case of the low fluence test at Rikkyo, the neutron fluence Φ_{eq} was determined from the leakage current of a reference diode. The fluence at the stripixel sensor was estimated to be $1.4 \times 10^{11} \text{ Neq/cm}^2$ using the inverse distance-squared dependence. On the other hand, the estimation in the high

fluence test at Tsukuba required a geometrical correction due to the Gaussian shape of the beam profile. The procedure to obtain the correction factor is as follows.

In order to measure the beam profile at the stripixel sensor, a plane Cu foil without a rectangular opening was irradiated at the same location as that of the test stripixel sensor. The proton beam had the same energy and the same intensity distribution. After the irradiation was over, the activated Cu foil ($^{63}\text{Zn}^*$) was taken out from the chamber and was laid on an imaging plate (IP) to transfer the intensity map. The IP is a 2-dimensional radiation recording device, which can be read out by scanning laser stimulated luminescence. (10) Fig. 10 shows the intensity distribution of the proton beam measured with the IP. The shape of the distribution was found to be consistent within a few percent with the calculated beam spread by Coulomb multiple scattering.

We evaluated the average fluence for the whole stripixel sensor area using the measured distribution. The average fluence of the stripixel sensor was 93% of that of the beam center, while that of the reference diode was 73%. The fluence at the stripixel sensor was finally determined to be $2.4 \times 10^{11} \text{ Neq/cm}^2$ by taking into consideration the ratio of the average fluences measured and the hardness factor 3.0 for 16 MeV protons. While the relative intensity of the activation was determined with the IP measurement, the absolute number of protons which irradiated the stripixel sensor was estimated in the following way.

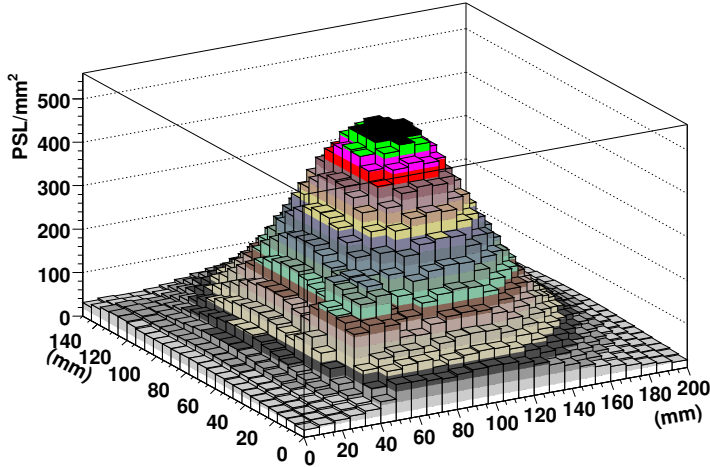


Fig. 10. Measured intensity distribution of the proton beam in Tsukuba test. Unit of PSL is proportional to the number of ^{63}Zn .

The Cu foil which was irradiated behind the test stripixel sensor was taken out from the chamber and the γ ray intensity was measured with a germanium (Ge) detector. The γ ray spectrum of activated foil had three main energy peaks at 669 keV, 962 keV and 1412 keV. The fluence was calculated by the following equation.

$$\Phi = \frac{N_\gamma \lambda T_r}{\epsilon B \sigma N_{Cu} d \Omega A} \quad (9)$$

$$A = (1 - \exp(-\lambda T_r))(\exp(-\lambda t_1) - \exp(-\lambda(t_1 + t_2))) \quad (10)$$

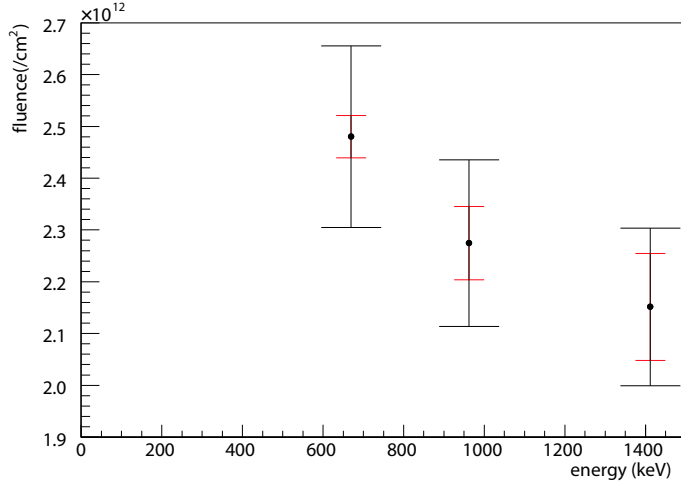


Fig. 11. Fluence of the Cu foil. Red line shows statistical error, black line shows systematic error.

where N_γ is the number of γ rays at one of the energy peaks, λ is the decay constant, T_r is irradiation time, ϵ is the detection efficiency, B is the branching ratio of the γ ray, σ is the activation cross-section, N_{Cu} is the number of ^{63}Cu atoms, $d\Omega$ is the solid angle of a gamma ray detector, t_1 is start time of measurement of γ rays and t_2 is the measurement time. The Ge energy calibration and the detection efficiency determination were done using standard checking sources. The solid angle was calculated from the source distance and the size of the detector sensitive area. The fluence determined at each energy peak is shown in Fig. 11. The values are all consistent with the fluence determined by the reference diode when both statistical and systematic errors are considered.

5.3. Leakage current of stripixel sensor

Fig. 12 shows IV/CV measurement result of the stripixel sensor irradiated with 14 MeV neutrons. The increase of leakage current is defined as difference between the pre-irradiation and post-annealing leakage current at V_{FD} and $T = 20^\circ\text{C}$. The measurement results are summarized in Table 4. It should be emphasized that the fluence determined by stripixel sensor was consistent with reference diode measurement within 10%. Also note that the consistency was confirmed between different kinds of radiation, namely 14 MeV neutrons and 16 MeV protons.

6. Test at PHENIX IR

In order to better understand the radiation that the stripixel sensors will be exposed to during RHIC II operations and the resultant possible damage, we performed a detailed measurement of the radiation dose in the PHENIX IR (Interaction Region) during the RHIC proton-proton run in 2006 (Run 6).

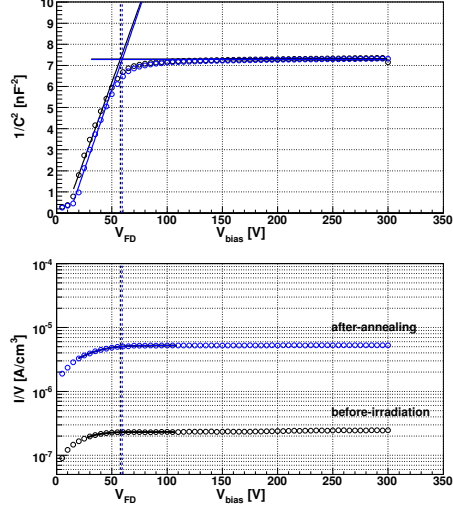


Fig. 12. IV/CV measurements for stripixel sensor irradiated with 14 MeV neutron beam.

Table 4

Beam test result with stripixel sensors.

stripixel sensor thickness [μm]	625	625	500
Beam particle	neutron	proton	proton
Beam energy [MeV]	14	16	200
$\Delta I/\text{Volume}$ [A/strip]	3.57×10^{-9}	7.39×10^{-8}	5.93×10^{-8}
$\Delta I/\text{Volume}$ [A/cm ³]	4.76×10^{-6}	9.86×10^{-5}	9.88×10^{-5}
Error $\Delta I/\text{Volume}$ [A/cm ³]	1.21×10^{-7}	6.04×10^{-7}	9.88×10^{-6}
α [A/cm]	4.04×10^{-17}	4.30×10^{-17}	4.00×10^{-17}
Fluence (reference diode) [N_{eq}/cm^2]	1.37×10^{11}	2.46×10^{12}	3.47×10^{12}
Fluence (neutron counter) [N_{eq}/cm^2]	1.88×10^{11}	-	-
Fluence (activation method) [N_{eq}/cm^2]	-	2.37×10^{12}	-
Fluence (beam monitor) [N_{eq}/cm^2]	-	-	5×10^{12}

Thirty thermoluminescent dosimeters (TLDs), sixteen pin diodes, two stripixel sensors, five temperature loggers, two C-AD personnel radiation monitoring instruments (chipmunks) and three beam loss monitors (BLMs) were installed at the PHENIX IR area, at various radii underneath the interaction point for the measurement of the instant and accumulated radiation dose during Run 6. Figure 13 shows the position of the radiation measurement structure underneath the beam pipe in the IR area of PHENIX.

The top strip of the structure was positioned 10 cm away from the beam pipe and ran parallel to the beam line. A set of 12 TLDs was placed on the top strip and six TLDs were positioned on the poletips of the PHENIX central magnet (see Fig. 13), three on the north side and three on the south, at radii where the vertex detector electronics will be positioned (5.08 cm, 10.16 cm, 15.24 cm). They were used to measure integrated dose and

study extensively the radial dependence of the dose. The pin diodes and stripixel sensors were placed on the top strip and used to measure the actual effect in units of equivalent 1 MeV neutron fluence, which is relevant to a silicon device. Two thermocouples and three thermochrons were positioned near the stripixel sensors to monitor the temperature during the irradiation period. The chipmunks were used to measure instantaneous dose and radial dependence of the radiation. The information from the chipmunks and the TLDs was then used to get RHIC II scaling factors and thus accordingly scale the stripixel sensors and pin diodes current measurements. The beam loss monitors are not sensitive enough to respond to the radiation from normal RHIC operation. They could detect potential acute radiation. Figure 14 shows the position of the BLMs and chipmunks in the radiation measurement mounting stand, as well as the sixteen pin-diodes and two stripixel sensors on the top strip. In further discussions the north-south axis, that runs parallel to the beam line, will be referred as the z axis.

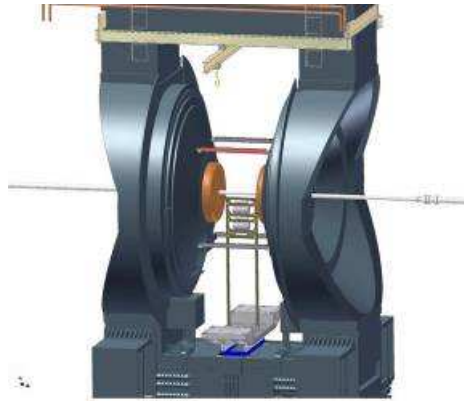


Fig. 13. Position of the radiation measurement structure underneath the beam pipe between the poletips of the PHENIX central magnet in the PHENIX IR.

6.1. TLDs

The TLDs were used to measure the accumulated radiation for the duration that the structure was in the IR. They were positioned close to the stripixel sensors and on the chipmunks and BLMs to cross-check the measurements from these devices.

6.1.1. TLD measurements - Dependence on radial distance from the beam line

The measurements from a number of TLDs placed at the same position along the beam axis, namely directly underneath the interaction point, were used to obtain the radial dependence R of the radiation from the beam line. In Figure 15 the TLD radiation measurements (red points) are plotted versus their distance R from the beam line and fit to the function $p_0 * R^{p_1}$. The estimated R dependence from the fit is -1.788 ± 0.047 .

Also six TLDs were placed on the magnet nose cones which are at 41 cm (south) and 41 cm (north) along the beam line (z -axis). These TLDs were left in the Interaction Region for the duration of the run (total luminosity $42pb^{-1}$) as opposed to the TLDs on

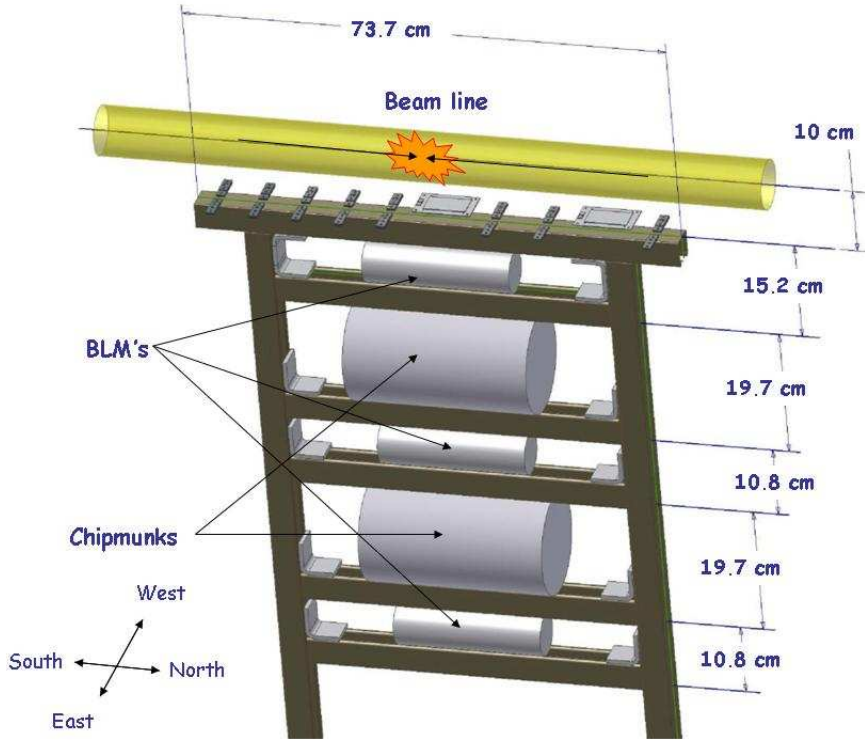


Fig. 14. Position of the BLMs and chipmunks in the mounting stand with the top strip placed 10 cm underneath the beam pipe

the strip and the ones attached at the BLMs and chipmunks that were in the area only for part of the run with a delivered luminosity of $12pb^{-1}$. Therefore the accumulated radiation values for these TLDs are higher. The measurements from these TLDs indicate a dependence on the distance from the beam line that is accordance with the radial dependence in Figure 15. In Figure 15 the nose cone TLD values (blue points), scaled at $12pb^{-1}$, have been overlaid with the values of the rest of the TLDs (red points).

6.1.2. TLD measurements - Dependence on distance from the Interaction Point along the beam line

A set of twelve TLDs placed on the strip that run parallel to the beam line (z axis) is used to study the dependence of radiation on z position.

In Figure 16 the TLD measured doses have been plotted with respect to their position along the beam axis. No obvious trend was observed.

6.2. Stripixel Irradiation

The sixteen pin diodes and two stripixel sensors were irradiated at radial distance 10 cm from the beam line in the PHENIX IR in Run 6. This will be the actual position of the stripixel sensors in the third layer of the VTX array. The center axis of the top

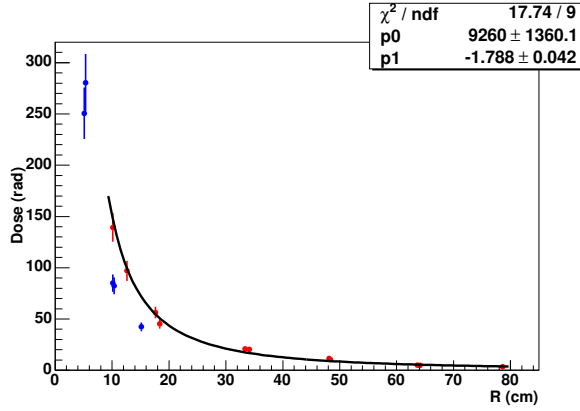


Fig. 15. Red points: TLD radiation measurements versus their distance R from the beam line and fit to the function $p0 * R^{p1}$. Blue points: TLDs placed on the nose cone, scaled to the same luminosity as the red points, versus their distance R from the beam line

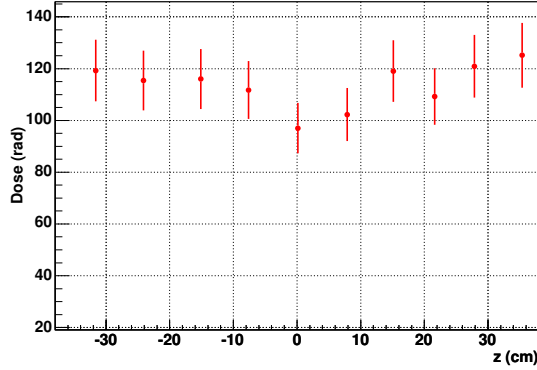


Fig. 16. TLD measured doses versus their positions along the beam axis.

strip was offset by 2 cm from the beam line so that one of the stripixel sensors would be directly underneath the interaction point. However the stripixel sensor placed underneath the interaction point was mechanically damaged so we only have results from one of the sensors.

There were two kinds of reference diodes with different volumes which were 0.01 cm^3 and 0.004 cm^3 . The increase of the leakage current of the diodes and the relevant fluences are summarized in Table 5. The average fluence of the diodes was $1.0 \times 10^{10} \text{ Neq/cm}^2$. The estimated z dependence of the diode fluence is shown in Fig. 17 which is in agreement with the TLDs.

The sensor was irradiated at $Z=25.2 \text{ cm}$ for about 50 days and the integrated luminosity during this time was 12 pb^{-1} . The current related damage rate α was estimated to be $3.2 \times 10^{-17} \text{ A/cm}$ using the temperature history of the temperature loggers in the PHENIX IR. The increase of leakage current of a single strip was $2.2 \times 10^{-10} \text{ A/strip}$ as seen in Table 5. Figure 18 shows the IV and CV measurements, where the leakage current and capacitance were measured before and after irradiation. The fluence of irradiated

stripixel sensor was estimated to $9.4 \times 10^9 \text{ N}_{eq}/\text{cm}^2$ which is consistent with the average fluence of the reference diodes.

Table 5

Increase of leakage current of irradiated stripixel sensor and diodes at R=10 cm in PHENIX IR.

	Z-distance (cm) [cm]	$\Delta I/\text{Volume}$ [A/cm ³]	Error $\Delta I/\text{Volume}$ [A/cm ³]	Fluence [N _{eq} /cm ²]	Error Fluence [N _{eq} /cm ²]
diode 1	33.5	4.5×10^{-7}	5.6×10^{-8}	1.4×10^{10}	1.8×10^9
diode 2	33.5	3.1×10^{-7}	5.7×10^{-8}	9.7×10^9	1.8×10^9
diode 3	16.8	2.1×10^{-7}	6.8×10^{-8}	6.7×10^9	2.1×10^9
diode 4	8.9	2.5×10^{-7}	8.1×10^{-8}	7.7×10^9	2.5×10^9
diode 5	8.9	2.8×10^{-7}	7.6×10^{-8}	8.7×10^9	2.4×10^9
diode 6	-7.1	2.1×10^{-7}	7.5×10^{-8}	6.4×10^9	2.3×10^9
diode 7	-7.1	2.5×10^{-7}	4.9×10^{-8}	7.7×10^9	1.5×10^9
diode 8	-13.7	2.3×10^{-7}	1.2×10^{-7}	7.0×10^9	3.9×10^9
diode 9	-13.7	3.1×10^{-7}	5.6×10^{-8}	9.5×10^9	1.7×10^9
diode 10	-20.3	3.5×10^{-7}	1.3×10^{-7}	1.1×10^{10}	3.9×10^9
diode 11	-20.3	2.6×10^{-7}	8.1×10^{-8}	8.0×10^9	2.5×10^9
diode 12	-26.9	3.6×10^{-7}	7.4×10^{-8}	1.1×10^{10}	2.3×10^9
diode 13	-26.9	4.1×10^{-7}	6.9×10^{-8}	1.3×10^{10}	2.2×10^9
diode 14	-33.5	5.3×10^{-7}	5.3×10^{-8}	1.7×10^{10}	1.7×10^9
stripixel sensor	25.2	3.0×10^{-7}	2.5×10^{-8}	9.4×10^9	7.8×10^8

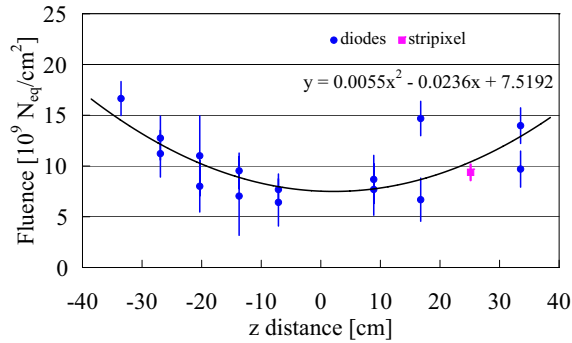


Fig. 17. Fluence of irradiated stripixel sensor and diodes at R=10 cm in PHENIX IR.

6.3. Chipmunks

The chipmunks provide a sensitive way to monitor the instantaneous rate of radiation in the IR. They are configured to read in dose equivalent units, i.e. “mrem/hr” on a meter.

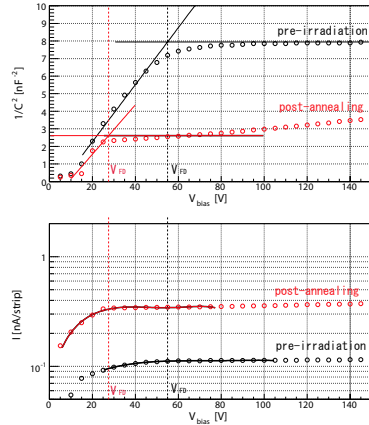


Fig. 18. IV/CV measurements result by stripixel sensor in PHENIX IR.

There is also an accompanying frequency output (Hz) that is proportional to the meter reading, calibrated with the use of a test source Cs-137. C-AD personnel determined that for Chipmunk 1 (positioned at 63 cm distance from the beam pipe) $4.68 \text{ Hz} = 42 \text{ mrem/hr}$, and for Chipmunk 2 (positioned at 33 cm distance from the beam pipe) $4.86 \text{ Hz} = 43 \text{ mrem/hr}$. In order to convert the dose equivalent measured by the chipmunks to absorbed dose in units of rad we have to use the following formula:

$$\text{Dose Equivalent (rem)} = \text{Absorbed Dose (rad)} \times \text{Quality Factor.} \quad (11)$$

The currently accepted value of the quality factor $Q.F. = 2.5$ for the RHIC environment was also assigned at PHENIX. Thus, the overall conversion from the frequency output to absorbed dose were determined to be $1 \text{ counts/sec} = 1 \mu\text{rad/sec}$ for Chipmunk 1 and $1 \text{ counts/sec} = 0.99 \mu\text{rad/sec}$ for Chipmunk 2. It should be noted that the accuracy of the quality factor is not important for this study since only ratios of chipmunk rates are used for the determination of the radial and luminosity dependence of dose. The doses obtained with the chipmunks were found to be consistently higher than that from the TLDs that were placed on them. This could be due to the different normalizations for converting the measurements in rads for the two kinds of devices. For example the TLDs do not get normalised to account for neutron radiation (12).

As seen in Figure 19 the chipmunk rates shape for a typical RHIC store is very similar to the PHENIX zero degree calorimeter (ZDC) (11). The initial structure (from 04/08/06 15:30 to 04/08/06 15:47) corresponds to the ramping, steering of the beams in the collider rings and then the peak during the time 15:47 to 16:00 corresponds to beam collisions having started but prior to the collimation of the beams. The spike in ZDC as well as the chipmunk corresponds to the ions in the periphery of the beams interacting with each other. Once the beams have been collimated the beam “halo” is reduced so the radiation dose goes down.

6.3.1. Dose dependence on radial distance from the interaction point

The measurements from the two chipmunks can be used to quantify the radial dependence of the absorbed radiation. In Figure 20 the ratio

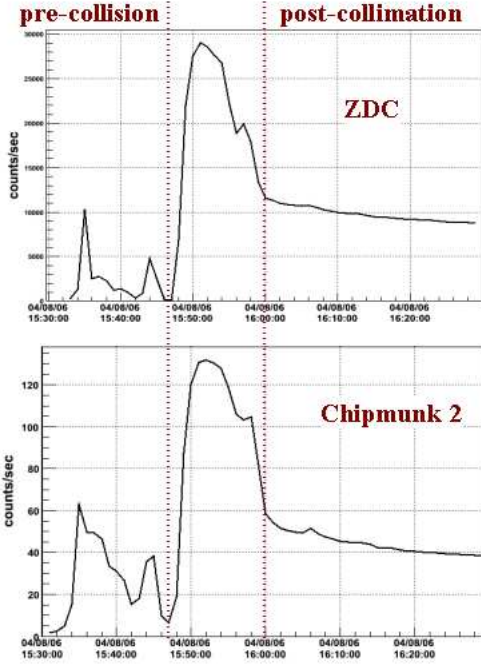


Fig. 19. Top: ZDC rate during a typical RHIC store. Bottom: Chipmunk 2 rate during the same store.

$$R_{radii} = \frac{\ln(C2/C1)}{\ln(R2/R1)} \quad (12)$$

for a typical store is plotted, where $C2$, $C1$ are the measured rates converted in $\mu\text{rad}/\text{sec}$ at Chipmunk 2 and Chipmunk 1 respectively and $R2$, $R1$ the distance of Chipmunk 2, Chipmunk 1 ($R2=33$ cm, $R1=63$ cm) from the beam pipe. The ratio for the post-collimation phase (Figure 20) indicates a radial dependence of $1/r^{1.83}$ where r is the distance from the beam line, which is in agreement with the R dependence obtained by the TLDs (-1.788 ± 0.047). The reason for the deviation from $1/r^2$, which would imply a point-like source, is an effect of the PHENIX magnetic field. This was verified with a zero field run shown in Fig. 21.

For the pre-collimation phase the radial dependence is greater than $1/r^3$ but less than $1/r^4$ as seen in Figure 20.

6.3.2. Scaling of Dose with Luminosity

In order to estimate the radiation dose during RHIC II we should examine the dependence of the dose on the delivered luminosities. If the post-collimation radiation is primarily due to collisions, then we can extrapolate the currently received dose to RHIC II according to the expected luminosities. Thus we examine whether the dose scales with luminosity by measuring the dose/luminosity variation from store to store. The luminosity is calculated as described in (13). In Figure 22 the dose/luminosity ratio (D/L) in $\mu\text{rad}/\text{mb}^{-1}$ for Chipmunk 2 indicates that the Dose scales with luminosity after collima-

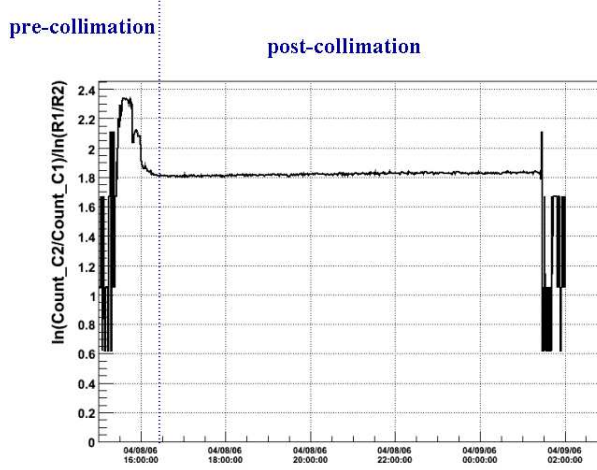


Fig. 20. Ratio $R_{rad} = \frac{\ln(C2/C1)}{\ln(R2/R1)}$, where $C2$, $C1$ are the measured rates for Chipmunk 2 and Chipmunk 1 respectively and $R2$, $R1$ the distance of Chipmunk 2, Chipmunk 1 from the beam pipe.

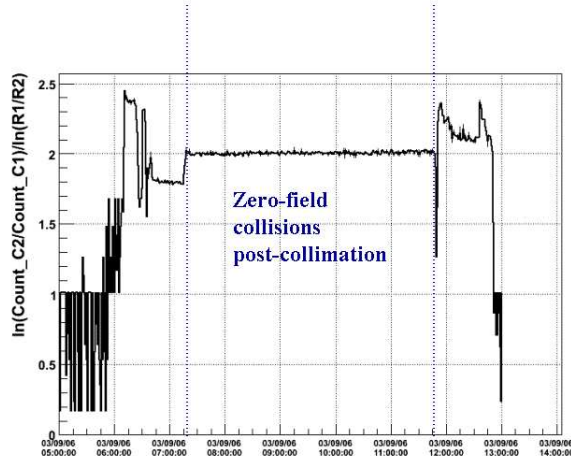


Fig. 21. Ratio $R_{rad} = 2$ for a zero field run - the post-collimation phase is indicated by the blue vertical lines.

tion. The ratio D/L is almost constant across all stores (with the luminosity increasing almost by a factor of two) and is $D/L = 1.500 \pm 0.075 \text{ rad/pb}^{-1}$ at 33 cm.

We confirmed that the post-collimation dose during Run 6 is mostly due to collisions by recording rates while C-AD personnel uncogged the beams, at our request. Namely, they altered the phase of the beams, so the ion bunches did not arrive at the collision points at the same time. Therefore, during the uncogged phase no collisions took place and the chipmunks recorded only 15% of the dose they recorded during the cogged phase.

We can estimate the total post collimation dose that was received during the current

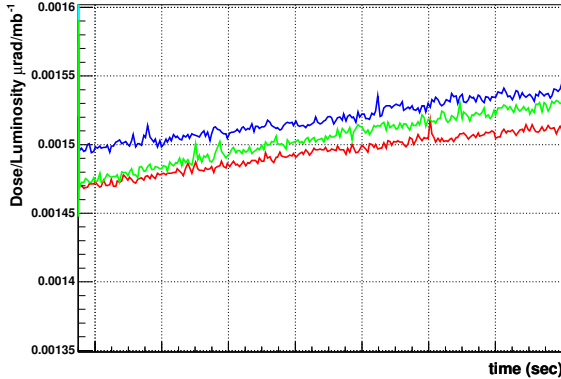


Fig. 22. Dose/Luminosity ratio in $\mu\text{rad}/\text{mb}^{-1}$ for Chipmunk 2, for a few typical stores

run by using the observed $D/L = 1.5 \text{ rad}/\text{pb}^{-1}$. The total delivered luminosity while the radiation measurement structure was in the IR, is 12 pb^{-1} and therefore the total estimated post collimation dose is 18 rad. The total dose (pre collimation, post collimation and aborted stores) that the Chipmunk 2 measured at 33 cm was 29.6 rad. Thus at Run 6, the dose due to collisions is

$$\frac{D_{\text{collision}}}{D_{\text{total}}} = 61\% \quad (13)$$

of the total received dose. The pre-collimation phase dependence on beam intensity was studied and the beam quality variations from store to store were such that if any such correlation exists it cannot be observed presently. The average store during the current run has a 0.08 rad/store radiation dose at 33 cm with a variation factor bigger than two. The total received pre-collimation dose was 5 rad and aborted stores contributed 7 rad to the total dose recorded by the chipmunks.

6.3.3. Projection to RHIC II according to the current PHENIX study

Having established the dependence of the radiation dose on luminosity and radial distance from the beam line, we can extrapolate our current measurements to the RHIC II running conditions and estimate the relevant dose expected.

The radiation dose received at a point of radial distance R from the interaction point, for two species colliding with center of mass energy E should be proportional to the number of particles produced during the collisions. In other words it should be proportional to the particle yield (dN/dy) for proton-proton collisions at rapidity $y=0$ for the relevant collision energy and the number of interactions occurring. If L is the luminosity delivered, σ the hadronic cross section at the relevant energy and N_{part} the number of participants for the species colliding then the Dose D is

$$D \propto \left(\int L \times \sigma dt \right) \times \left(\frac{dN}{dy} \right)_{pp} \times N_{\text{part}} \times \left(\frac{1}{R} \right)^{1.83} \quad (14)$$

Forming the ratio of the doses D_A , D_B in two different states A and B:

$$\frac{D_B}{D_A} = \frac{L_B * N_{part_B} * \sigma_B * \left(\frac{dN}{dy}\right)_B}{L_A * N_{part_A} * \sigma_A * \left(\frac{dN}{dy}\right)_A} \times \left(\frac{R_A}{R_B}\right)^{1.83} \quad (15)$$

we can estimate the radiation dose that the stripixel sensors will receive after collimation at 10 cm, during RHIC II operations under the assumption that all the dose will be due to collisions. The total measured fluence for the stripixel sensor during Run 6 was $9.4 \cdot 10^9 N_{eq}/cm^2$, as mentioned in Section 6.2. However the dose due to collisions should be $0.61 \times 9.4 \cdot 10^9 N_{eq}/cm^2 = 5.7 \cdot 10^9 N_{eq}/cm^2$ according to formula 13.

In Table 6 there is a summary of the Run 6 PHENIX measurement for the stripixel sensor fluence and run conditions. Also the expected luminosities [1], cross sections and N_{part} for twenty week runs for a number of different species and collision energies at RHIC II. Since the purpose of this study is mainly to obtain the projection factors from the current dose received to RHIC II expected radiation dose, we report the ratio $Dose_B/Dose_A$, where $Dose_A$ is the measured fluence for the stripixel sensor at 10 cm for the current run and $Dose_B$ the expected dose for these 20 week runs, as well as the projected fluences.

For a ten year run, assuming one year of 500 GeV pp run and three years for each of other species (Au-Au, Cu-Cu, pp at 200GeV) the total expected post collimation dose at 10 cm would be $4.3 \cdot 10^{12} N_{eq}/cm^2$. We could also estimate an upper limit for the total radiation received by the stripixel sensors by using the total measured fluence, $9.4 \cdot 10^9 N_{eq}/cm^2$, which includes the pre-collimation, post collimation phases and aborted stores. If we use formula 15 and the total measured fluence then the expected radiation for a ten year run at RHIC II would be $7.4 \cdot 10^{12} N_{eq}/cm^2$. However a more realistic upper limit can be set by estimating the dose during the pre-collimation phase.

Similarly we can repeat these calculations using the chipmunk dose of 18 rad for $L = 12 \text{ pb}^{-1}$ at 33 cm. The expected post-collimation dose for RHIC II at 10 cm from the beam line is estimated to be 127 krad. For the pre-collimation dose, if we assume a scaling of $1/r^{-2.35}$, 500 stores per year and no dependence on beam intensity, then the projected dose at 10 cm for a ten year run of RHIC II would be :

Table 6

PHENIX measurement - post collimation at 10 cm for stripixel sensor								
Species	\sqrt{s} (GeV)	dN/dy at y=0	Npart	cross section (b)	radius (cm)	Luminosity (nb^{-1})	$Dose_A$ (krad)	fluence Φ_{eq} (N_{eq}/cm^2)
pp	200	3.6	2	$4.2 \cdot 10^{-2}$	10	$1.2 \cdot 10^4$		5.7×10^9
Projection at 10 cm for 20 week RHIC II runs								
Species	\sqrt{s} (GeV)	dN/dy at y=0	Npart	cross section (b)	radius (cm)	Luminosity (nb^{-1})	$Dose_B/Dose_A$	fluence Φ_{eq} (N_{eq}/cm^2)
pp	500	4	2	$4.7 \cdot 10^{-2}$	10	$3.3 \cdot 10^6$	341.3	$1.9 \cdot 10^{12}$
pp	200	3.6	2	$4.2 \cdot 10^{-2}$	10	$7.0 \cdot 10^5$	58.2	$0.3 \cdot 10^{12}$
AuAu	200	3.6	100	7.0	10	$5.0 \cdot 10^1$	35.1	$0.2 \cdot 10^{12}$
CuCu	200	3.6	35	3.4	10	$5.0 \cdot 10^2$	58.9	$0.3 \cdot 10^{12}$

$$0.08\text{rad}/\text{store} \times 10\text{year} \times 500\text{stores}/\text{year} \times (33\text{cm}/10\text{cm})^{2.35} = 6.6\text{krad} \quad (16)$$

Thus the total (pre+post-collimation) expected radiation is 133.6 krad and the pre-collimation dose would be in the order of a 5% effect. Thus a more realistic upper limit for the expected fluence during 10 years of RHIC II operations would be $4.5 \cdot 10^{12} N_{eq}/\text{cm}^2$.

6.3.4. CDF fluence measurement

The CDF experiment at the Tevatron Collider at Fermilab has also measured the bulk radiation damage in silicon sensors and the dependence of 1MeV equivalent neutron fluence on the sensor radius from the beam and delivered luminosity (14). The radiation damage in the SVX and SVX' silicon vertex detectors was measured at 3 cm distance from the I.R. via their leakage currents. Their estimated equivalent 1MeV neutron fluence per fb^{-1} for pp collisions at 1.8 TeV is

$$2.19 \pm 0.63 \cdot 10^{13} r[\text{cm}]^{-1.68} n_{eq} \text{cm}^{-2} / fb^{-1} \quad (17)$$

It would be instructive to compare their measurement with our results for the stripixel sensor fluence. Using formula 15 but with the r-dependence that was observed at CDF ($r^{-1.68}$) we can project their measurement to our Run 6 conditions for the stripixel sensor placed at 10 cm from the beam line. In table 7 there is a summary of the PHENIX Run 6 conditions and measurement for the stripixel sensor fluence, the CDF run conditions and fluence measurement as well as the the estimated fluence for the PHENIX stripixel sensor at 10 cm according to the CDF measurement and radial dependence.

The PHENIX post-collimation fluence for the stripixel sensor $5.7 \pm 0.8 \cdot 10^9 N_{eq}/\text{cm}^2$ is somewhat higher than the CDF based estimation of $3.7 \pm 1 \cdot 10^9 N_{eq}/\text{cm}^2$ fluence at 10 cm from the beam line.

Table 7

PHENIX measurement - post collimation at 10 cm for stripixel sensor								
Species	\sqrt{s} (GeV)	dN/dy at y=0	Npart	cross section (b)	radius (cm)	Luminosity (nb^{-1})	fluence Φ_{eq} (N_{eq}/cm^2)	$\delta\Phi_{eq}$ (N_{eq}/cm^2)
pp	200	3.6	2	$4.2 \cdot 10^{-2}$	10	$1.2 \cdot 10^4$	$5.7 \cdot 10^9$	$0.8 \cdot 10^9$
CDF measurement								
Species	\sqrt{s} (GeV)	dN/dy at y=0	Npart	cross section (b)	radius (cm)	Luminosity (nb^{-1})	fluence Φ_{eq} (N_{eq}/cm^2)	$\delta\Phi_{eq}$ (N_{eq}/cm^2)
pp	1800	4.3	2	$5.2 \cdot 10^{-2}$	3	$1.0 \cdot 10^6$	$3.47 \cdot 10^{12}$	$1 \cdot 10^{12}$
CDF based estimation of fluence at 10 cm for PHENIX stripixel sensor								
Species	\sqrt{s} (GeV)	dN/dy at y=0	Npart	cross section (b)	radius (cm)	Luminosity (nb^{-1})	fluence Φ_{eq} (N_{eq}/cm^2)	$\delta\Phi_{eq}$ (N_{eq}/cm^2)
pp	200	3.6	2	$4.2 \cdot 10^{-2}$	10	$1.2 \cdot 10^4$	$3.7 \cdot 10^9$	$1 \cdot 10^9$

7. IUCF irradiation test

7.1. Introduction

As a part of the radiation damage tests, one pre-production wafer with 3 sensors and 6 test photo diodes were sent to the University of New Mexico (UNM) group for tests at their facility. The sensors were diced out of the wafer by Micro Dicing Technology Inc. in California. After all the necessary measurements were performed, the sensors were sent to IUCF for irradiation. Two sensors and two diodes were irradiated at the Indiana University Cyclotron Facility (IUCF), returned to UNM and post irradiation measurements were performed.

All the measurements presented were performed on a $500\mu\text{m}$ preproduction sensor with identification B2W15 sensor 1 (s1), sensor 2 (s2) and sensor 3 (s3). The sensors were fabricated by Hamamatsu Photonics/Japan. The number of readout strips per sensor is 128 strip-pixels per set of read-out pads \times 12 sets per sensor = 1536 strips [1].

The complete testing program consisted of visual inspection, mechanical measurements (flatness and warp), and electrical measurement. The electrical measurements consisted of the leakage current I_{Leak} and the capacitance C_{Strip} performed at a fixed bias voltage V_{Bias} on every channel out of a set of 128. These measurements determine the leakage current and capacitance values of the sensor and enable the identification of bad channels. The second set measures the leakage current and the capacitance versus bias voltage V_{Bias} . From these measurements the breakdown V_{Break} and the depletion voltage V_{Depl} are found. The breakdown voltage for all sensors to be $V_{Break} > 500V$. To find the bias voltage at which the bulk material is depleted of all free charge carriers, the capacitance is measured as a function of V_{Bias} and $1/C^2$ is plotted via V_{Bias} . The depletion voltage is found to be $V_{Depl} \simeq 95V$. To determine the leakage current and the capacitance of the sensor under fully depleted conditions, the current and capacitance are measured at an operating voltage of V_{oper} which is chosen as $V_{Depl} + 50V < V_{oper} < V_{Break}$. The operating voltage was chosen as 200V, putting the sensor well into the fully depleted region of operation but also far away from breakdown conditions. The measurements yielded characteristic plots for the leakage current and capacitance vs channel # as shown in fig.s (?) and (?).

The measurements of the leakage current I_{Leak} and capacitance C are performed on each set of 128 channels, 12 measurements per sensor, on each sensor. All the channels should have approximately the same amount of leakage current and capacitance. This is not the case as can be seen in figures (11) and (12). The first and the last 20 to 30 channels are not on a flat line, but show an increase in leakage current. This is due to these channels bordering the unbiased region of the sensor. This means that the parts of the sensor right next to the outside lying channels that are measured, are not depleted of free charge carriers, therefore increasing the leakage current in the channels that are closest to these regions. This situation was resolved as discussed in section 4.1. To get a measure of the leakage current, all the channels that were in the flat part of the curve, between channels 25 and 105 were used to calculate average Leakage current and Capacitance. In the following the same measurements were performed with the sensor fully depleted by wirebonding the unmeasured pads to the guardring. This led to major changes in the results. The left sides of s1 and s2 were grounded by connecting 5 out of the six set of

pads to the guardring which is connected to ground through the probecard. To make the wirebonds a wedge type wirebonder was used. The wires have a diameter of $25\mu m$ and are Aluminum 1% Silicon wires. The wedge has dimensions of $64\mu m$ by $102\mu m$. Due to the size of the wedge, the wirebonds were hard to make precisely, because the size of one pad is only $69\mu m$ by $104\mu m$. A different technique of connecting the pads to the guardring was used. By applying a graphite resistance coating (Aerodag G), a connection between the guardring and the pads was made. The graphite could be easily removed with alcohol after the measurements without damaging the sensor. The leakage current and the capacitance were determined as described before. This time, only two measurements per sensor contributed to the calculation of the average, as the other pads on the sensor were permanently connected to the guardring (not permanently in the case of the graphite, but the connections were not removed either). With these connections in place the typical change of the Leakage Current measurement can be seen in figure (16). This measurement shows the impact of the biasing of the whole sensor on the leakage current. Using all the five measurements taken, one obtains the following value for I_{Leak} :

$$I_{Leak,allbiased} = 3.6nA \quad , \quad \sigma_I = 3.9nA \quad (18)$$

$$I_{Leak,original} = 11.8nA \quad , \quad \sigma_I = 5.5nA \quad (19)$$

With this the average capacitance of the sensor is found to be

$$C_{allbiased} = 1.3pF \quad , \quad \sigma_C = 1.9pF \quad (20)$$

$$C_{original} = 1.7pF \quad , \quad \sigma_C = 0.3pF \quad (21)$$

Both of the values, for the leakage current and the capacitance, are a lot better defined than the previously measured. The leakage current at room temperature is small enough to leave room for irradiation damage (in the case that the detector is kept at 0C).

7.2. Radiation tests

The purpose of the radiation tests was to study the effects of radiation damage on the strip-pixel sensor. In particular on the breakdown voltage, the depletion voltage, the leakage current and the capacitance.

Two of the three available sensors and two of the six testdiodes were irradiated. The sensors/diodes were irradiated at the Indiana University Cyclotron Facility (IUCF) with 200MeV protons. The sensors as well as the diodes were completely emerged in the beam, as the IUCF has the capability to irradiate areas from less than 2cm to 30cm in diameter with a smaller then 30 percent variation of the radiation over the chosen area. The dosimetry at IUCF is routinely better than 10 percent ensuring the accuracy of the chosen doses. Further details of the irradiation are summarized in the following table.

	Irradiation Dose p/cm^2	n-equivalent dose
Sensor 1 / Diode 1U	$5 \cdot 10^{12}$	$4.945 \cdot 10^{12} \pm 4\%$
Sensor 2 / Diode 1D	$5 \cdot 10^{11}$	$4.945 \cdot 10^{11} \pm 4\%$

To calculate the 1MeV neutron equivalent radiation dose, the hardness factor $\kappa_{200MeV,p} = 0.989 \pm 4\%$ for 200MeV protons was used (?). The specific doses were chosen as they are a good estimate to the expected radiation dose that the detector will experience over the next ten years in RHIC and RHIC II. The irradiations were performed at room temperature and no bias was applied to the sensors and diodes during irradiation. After the irradiation, the sensors/diodes were kept in a -17° freezer, shipped to UNM in dry ice and again kept in a -20° freezer until measured. During the measurements a thermal chuck was used, keeping the sensors/diodes at about $-1^\circ C$. The diodes were measured first to use them as a control to find the actual fluence levels obtained during irradiation. IV measurements were made at $-1^\circ C$ and the results were normalized to $20^\circ C$ according to the equation $I(T) \propto T^2 \cdot e^{-\frac{E}{2kT}}$, where E is the effective energy gap, T is the measured temperature and k is Boltzmann's constant. To measure the diodes the probecard was replaced with a single probe (the scanner was not used) and IV and CV curves were measured. As before, V_{Break} was determined from IV and the CV measurements were used to find V_{Depl} . After the initial measurements the diodes were annealed at $60^\circ C$ for 80min and the measurements were repeated. The results from the annealed diodes are presented first, because they are used to identify the real equivalent flux from the results of the non annealed diodes.

Next the leakage current on the annealed diodes was measured. The damage parameter α after annealing at $60^\circ C$ for 80min is constant (?) at $\alpha_{80/60} = 4.0 \cdot 10^{-17} A/cm \pm 4\%$. Using the leakage currents at $V_{Bias} = 200V (> V_{Depl})$, the constant α and the Volume of the diodes ($Vol = 4mm \cdot 4mm \cdot 0.5mm \pm 10\%$), the equivalent fluences can be calculated using $\alpha = \frac{\Delta I}{Vol \cdot \Phi_{equ}}$. This gives the following values for the equivalent fluences

$$\Phi_{equ,1} = (4.251 \pm 0.458) \cdot 10^{11} cm^{-2} \quad (22)$$

$$\Phi_{equ,2} = (3.472 \pm 0.374) \cdot 10^{12} cm^{-2} \quad (23)$$

Φ_{proton} is then calculated via $\Phi_{proton} \cdot \kappa_{200MeV,p} = \Phi_{equ}$ and all the different fluences compare as follows

	Measured (cm^{-2})	Target (cm^{-2})	Irrad. Lab Dosimetry (cm^{-2})
$\Phi_{proton,1}$	$(4.298 \pm 0.494) \cdot 10^{11}$	$5.0 \cdot 10^{11}$	$5.004 \cdot 10^{11} \pm 10\%$
$\Phi_{proton,2}$	$(3.511 \pm 0.403) \cdot 10^{12}$	$5.0 \cdot 10^{12}$	$5.001 \cdot 10^{12} \pm 10\%$

These numbers will be used instead of the ones that were given by the irradiation Lab. Similarly to the diodes, the sensors were annealed for 80min at $60^\circ C$ and measurements were taken before and after annealing. This time, sensor 1, which was irradiated

to $5 \cdot 10^{12} \text{cm}^{-2}$, was not measured pre-annealing because the currents were too high and the thermal chuck used could only cool the sensor to -1°C . Therefore, only the measurements post annealing are discussed. To measure the sensors, all the readout pads were again biased. All the measurements were taken at 0°C for the $5 \cdot 10^{11} \text{cm}^{-2}$ sensor and at -10°C for the $5 \cdot 10^{12} \text{cm}^{-2}$ sensor, the IV results normalized to $+20^\circ\text{C}$. From the IV measurements it can be seen that the breakdown voltage for s2 ($5 \cdot 10^{11}$) is at

$$V_{Break} \simeq 280V$$

. The measurement for s2 stops at 280V, because the whole sensor breaks down at this voltage and exceeds the highest possible compliance limit on the ammeter. The same happens for s1 ($5 \cdot 10^{12}$) at $\sim 250V$. The difference for s1 is, that no rise in the IV curve is seen at 250V, so the breakdown voltage stays unknown for this sensor. The depletion voltage for s2 is

$$V_{Depl} \simeq 100V$$

and for the non-irradiated sensor

$$V_{Depl} \simeq 120V$$

. The depletion voltages obtained from a laser pulsing test are plotted versus the radiation fluence, shown in fig.(?). This result implies that the highly irradiated sensor went through type inversion, increasing the depletion voltage from the non irradiated sensor, while the sensor that was irradiated with the lower dose is still on the beneficial side of the annealing [3]. The leakage current measurements are plotted in fig.(29). The 20°C normalized leakage currents are found to be:

Radiation Dose	I_{Leak} (nA)
non irradiated	$\simeq 1.5$
$4.298 \cdot 10^{11} \text{cm}^{-2}$	$\simeq 4.3$
$3.511 \cdot 10^{12} \text{cm}^{-2}$	$\simeq 60.8$

When plotting I_{Leak} vs the radiation fluence, the slope of the line should be equal the damage parameter α divided by the volume under one strip Vol_{Strip} . This volume can be estimated and also found from the plot of Φ_{equ} vs $\Delta I/Vol$, because as the measurements were performed after annealing the sensors, α again has to be $4 \cdot 10^{-17} \text{A/cm}$. The volume under one strip is estimated as follows. One pixel has two spirals of p+ implant interleaving. They are identical to each other, but one is rotated by 180° with respect to the other. So half of the volume of one pixel should correspond to the volume of one pixel for one strip. The volume of one pixel is calculated from its width $w = 0.08 \text{mm}$, its length $l = 1 \text{mm}$ and its thickness of $d = 0.5 \text{mm}$. It also has to be considered that 30 pixels are connected together to give one strip-pixel, so the volume can be estimated as:

$$Vol_{strip,est} = \frac{1}{2} \cdot 0.08 \text{mm} \cdot 1 \text{mm} \cdot 0.5 \text{mm} \cdot 30 = 0.6 \cdot 10^{-4} \text{cm}^3 \quad (24)$$

Accounting for the gaps between the p+ implants, this value for the volume should approximately be divided by a factor of 2. Then the estimated volume will be

$$Vol_{strip,est} \simeq 0.3 \cdot 10^{-4} \text{cm}^3 \quad (25)$$

Using the calculated volume $Vol_{strip,calc}$, $\Delta I/Vol_{strip,calc}$ vs Φ_{eq} can be plotted to see if it corresponds to the universally found plot (?), shown in fig.(?). To a good approximation, the data points lie on the universal line, therefore confirming that the measurements agree with the universal idea.

The irradiation studies at UNM have showed that the preproduction strip-pixel sensors show an increase in leakage current as a function of the radiation damage which is consistent with expectations. These levels of increase in leakage current may be a problem for the electronics if the detector is not cooled during operation. The lack of bias resistors on the sensors makes meaningful testing problematic and should be considered for the final design.

8. Conclusion

In conclusion, we have reproduced the CERN-RD48 proportionality between Φ_{eq} and $\Delta I/Volume$ using their reference diodes in beam irradiation experiments. The CERN results were used to convert $\Delta I/Volume$ of the reference diode to 1 MeV neutron equivalent fluence Φ_{eq} in our irradiation experiments.

PHENIX VTX silicon stripixel sensors were irradiated along with reference diodes using neutron and proton beams with various fluences. We found the same behavior also holds for the stripixel sensor.

A stripixel sensor installed in the PHENIX experimental hall during the run period in 2006 was exposed to the radiation coming from proton-proton collisions at $\sqrt{s} = 200$ GeV at 10 cm away from the beam line. The correspondence between integrated luminosity of RHIC for pp collisions and Φ_{eq} at 10 cm was determined. The conversion factor was found to be $\Phi_{eq}/pb^{-1} = 8 \times 10^8 \text{ N}_{eq}\text{cm}^{-2}/pb^{-1}$.

Fig. 23 is the summary plot of the stripixel sensor results as a function of Φ_{eq} determined by reference diode at 20 °C. All data points are in agreement with the CERN-RD48 results; Eq. (1).

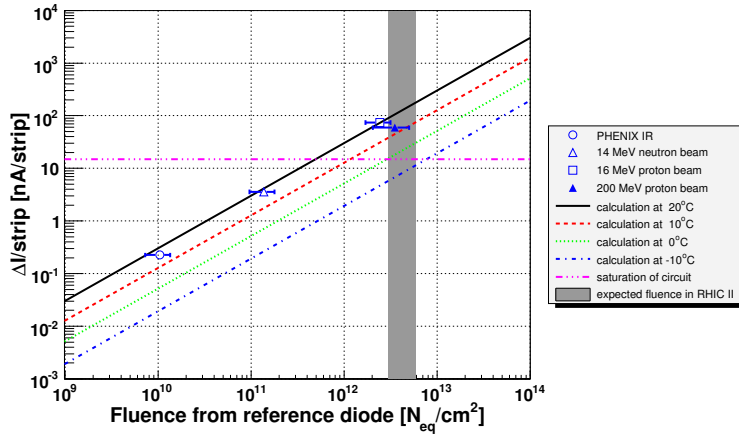


Fig. 23. Dependence of leakage current for stripixel sensor on irradiated fluence determined with reference diode.

The estimated integrated luminosity of RHIC II runs for 10 years is $4 fb^{-1}$, which translates to $\Phi_{eq} = 3.6 \times 10^{12} N_{eq}/cm^2$ (gray band in Fig. 23). Though the expected leakage current exceeds the required limit of 15nA/channel at 20 °C, we can suppress the leakage current by lowering the operating temperature. It is concluded that the stripixel sensors need to be operated at $T \leq 0$ °C.

acknowledge here. we will write.

References

- [1] K. Adcox et al., Nucl. Instr. and Meth. A499 (2003) 469.
- [2] K. Adcox et al., Nuclear Physics A757 (2005) 184.
- [3] Y. Akiba, et al., Proposal for a Silicon Vertex Tracker (VTX) for the PHENIX Experiment (Brookhaven National Laboratory, Upton, NY, 2005)
- [4] S.S. Adler et al., Phys. Rev. Lett. 93 (2004) 202002.
- [5] Z. Li, et al., Nucl. Instr. and Meth. A 518 (2004) 300-304, A 518 (2004) 738-753, A 535 (2004) 404-409, A 541 (2005) 137-143
- [6] B. Krieger, et al.: IEEE Trans. Nucl. Sci. **51** 1968 (2004).
- [7] S. M. Sze and Kwon K. Ng, Physics of Semiconductor Devices, Wiley Published 2006/10
- [8] A. Vasilescu (INPE Bucharest) and G. Lindstroem (University of Hamburg), Displacement damage in silicon, on-line compilation
- [9] M. Moll, Ph.D. Thesis, University of Hamburg, 1999, DESY THESIS-1999-040, ISSN-1435-8085
- [10] Sonoda M, Takano M, Migahara J, Kato H. Computed radiography utilizing scanning laser stimulated luminescence. Radiology. 1983;148:833-838.
- [11] S. Adler et al., Nucl. Instrum. Meth A461:337-340, 2001.
- [12] Private communication with Landauer.
- [13] S.Belikov, G.Bunce, M. Chiu, K.A. Drees, B.Fox, Y.Goto, T.Kawabata, N.Saito, H.Sato, and M. Tannenbaum.
Determination of the Absolute Luminosity for the Proton-Proton Data at $\sqrt{s}=200$ GeV Recorded by PHENIX during RHIC Run-02, analysis note 184.
- [14] John A.J. Matthews Effective Silicon Damage Fluences measured by SVX and SVX' CDF Note 3937